

Light Gradient Boosting Machine as a Regression Method for Quantitative Structure-Activity Relationships

Robert P. Sheridan ¹, Andy Liaw, ²Matthew Tudor ³

1. Computational and Structural Chemistry, Merck & Co. Inc., Kenilworth, NJ, U.S.A. 07033
2. Biometrics Research Department, Merck & Co. Inc., Rahway, NJ, U.S.A. 07065
3. Computational and Structural Chemistry, Merck & Co. Inc., West Point, PA, U.S.A 19486

sheridan@merck.com

ORCHID

Sheridan 0000-0002-6549-1635

Liaw 0000-0002-2233-7427

Tudor 0000-0001-8766-195X

ABSTRACT

In the pharmaceutical industry, where it is common to generate many QSAR models with large numbers of molecules and descriptors, the best QSAR methods are those that can generate the most accurate predictions but that are also insensitive to hyperparameters and are computationally efficient. Here we compare Light Gradient Boosting Machine (LightGBM) to random forest, single-task deep neural nets, and Extreme Gradient Boosting (XGBoost) on 30 in-house data sets. While any boosting algorithm has many adjustable hyperparameters, we can define a set of standard hyperparameters at which LightGBM makes predictions about as accurate as single-task deep neural nets, but is a factor of 1000-fold faster than random forest and ~4-fold faster than XGBoost in terms of total computational time for the largest models. Another very useful feature of LightGBM is that it includes a native method for estimating prediction intervals.

INTRODUCTION

Quantitative Structure-Activity Relationships (QSAR) models are very useful in the pharmaceutical industry for predicting on-target and off-target activities. While higher prediction accuracy is desirable, computational efficiency is also important. In an industrial environment there may be a dozens of models trained on a very large number ($>100,000$) of compounds and a large number (several thousand) of substructure descriptors. These models may need to be updated frequently (say, every few weeks). QSAR methods that are particularly compute-intensive or require the adjustment of many sensitive hyperparameters to achieve good prediction for an individual QSAR data set are therefore less desirable. Other useful characteristics of a good method include the ability to make predictions rapidly, produce interpretable models, and indicate how reliable each prediction might be.

Random forest (RF) (Breiman, 2001; Svetnick et al., 2003) was attractive as a QSAR method for many years because it is easily parallelizable and has few adjustable hyperparameters, as well as being relatively accurate in prediction. The most notable recent trend in the QSAR literature is the use of deep neural nets (DNN) (Gawehn et al., 2016), starting with our original work stemming from our Kaggle competition (Ma et al, 2015). On the plus side, DNNs tend to make very accurate predictions. On the other hand, DNNs tend to be computationally expensive and their models are not easily interpretable. Gradient boosting is another interesting QSAR method that has undergone rapid development. We investigated Extreme Gradient Boosting (XGBoost) by Chen and Guestrin (2016) on QSAR problems (Sheridan et al., 2016). Later we examined BART (Feng et al., 2019). While boosting methods have a very large number of adjustable hyperparameters, we can show that, in certain ranges, predictivity is at a near maximum and one can pick a standard set of hyperparameters for XGBoost with which most QSAR problems can achieve a level of prediction about as good as DNN, with much less computational expense.

Recently a new method of gradient boosting called Light Gradient Boosting (LightGBM) has appeared (Ke et al., 2017). LightGBM differs from XGBoost in a few aspects. We will only discuss the ones that are relevant in the context of QSAR. In XGBoost, trees are grown to a pre-specified depth; i.e., it will not split nodes to the $k+1$ -st level until it had performed all possible splits at the k -th level. LightGBM, on the other hand, will split the node that maximizes the drop in the loss function (thus it can grow “lop-sided” trees). This is the “best-first” strategy of regression tree induction described in Friedman (2001). (This feature has also recently been added to the XGBoost software as an option.) In addition, LightGBM introduced a feature, “exclusive feature bundling”, which collapse sparse descriptors (those with very few non-zero elements, and the non-zero elements do not occur in the same molecules) into one feature. This not only increase the computational efficiency, but can increase the information content of descriptors seen by the algorithm. There are other features in LightGBM that increase the computational efficiency in terms of time and memory usage.

One feature of LightGBM that was not in the original formulation of XGBoost is a method for assigning uncertainty of predictions. Uncertainty of predictions can be estimated via prediction intervals; i.e., the interval (L, U) should have 95% chance of containing the measured activity. The wider the interval (U – L), the higher the uncertainty in the prediction. LightGBM can be used to estimate these intervals by using a quantile loss function.

Several groups have compared boosting methods on a number of machine learning applications. The claim for general machine learning problems is that LightGBM is much faster than XGBoost and takes less memory (Omar, 2017; Anghel et al. 2019; Du et al., 2019). A recent paper by Zhang et al. (2019) applies LightGBM to classification problems, specifically to toxicity and compares its performance to RF, DNN, and XGBoost in random cross-validation. This paper compares LightGBM against RF, DNN, and XGBoost as a regression method for prospective prediction on a wider variety of QSAR problems. We can show that a subset of hyperparameters can be found at which LightGBM is faster than XGBoost and achieves prediction accuracies equivalent to single-task DNN. We also examine the prediction intervals from LightGBM in comparison to RF and BART.

METHODS

Data sets

Table 1 shows the in-house data sets used in this study which are the same as in Ma et al. (2015) and Sheridan et al. (2016). These data sets represent a pharmaceutical research relevant mixture of on-target and off-target activities, easy and hard to predict activities, and large and small data sets. Descriptors for the data sets (in disguised form) are available in Supporting Information of Sheridan et al. (2020). As before, we use in-house data sets because:

1. We wanted data sets which are realistically large, and whose compound activity measurements have a realistic amount of experimental uncertainty and include a non-negligible amount of qualified data.
2. Time-split validation (see below), which we consider more realistic than any random cross-validation, requires dates of testing, and these are very hard to find in public domain data sets.

Table 1. Data sets for prospective prediction.

Data set	Type	Description	Number of Molecules Training+test	Number of unique AP,DP descriptors	Mean \pm stdev activity
2C8	ADME	CYP P450 2C8 inhibition -log(IC50) M	29958	8217	4.88 \pm 0.66
2C9BIG	ADME	CYP P450 2C9 inhibition -log(IC50) M	189670	11730	4.77 \pm 0.59
2D6	ADME	CYP P450 2D6 inhibition -log(IC50) M	50000	9729	4.50 \pm 0.46
3A4*	ADME	CYP P450 3A4 inhibition	50000	9491	4.69 \pm 0.65

		-log(IC50) M			
A-II	Target	Binding to Angiotensin-II receptor -log(IC50) M	2763	5242	8.70±2.72
BACE	Target	Inhibition of beta-secretase -log(IC50) M	17469	6200	6.07±1.40
CAV	ADME	Inhibition of Cav1.2 ion channel	50000	8959	4.93±0.45
CB1*	Target	Binding to cannabinoid receptor 1 -log(IC50) M	11640	5877	7.13±1.21
CLINT	ADME	Clearance by human microsome log(clearance) µL/min/mg	23292	6782	1.93±0.58
DPP4*	Target	Inhibition of dipeptidyl peptidase 4 -log(IC50) M	8327	5203	6.28±1.23
ERK2	Target	Inhibition of ERK2 kinase -log(IC50) M	12843	6596	4.38±0.68
FACTORXIA	Target	Inhibition of factor Xla -log(IC50) M	9536	6136	5.49±0.97
FASSIF	ADME	Solubility in simulated gut conditions log(solubility) mol/l	89531	9541	-4.04±0.39
HERG	ADME	Inhibition of hERG channel -log(IC50) M	50000	9388	5.21±0.78
HERGBIG	ADME	Inhibition of hERG ion channel -log(IC50) M	318795	12508	5.07±0.75
HIVINT*	Target	Inhibition of HIV integrase in a cell based assay -log(IC50) M	2421	4306	6.32±0.56
HIVPROT*	Target	Inhibition of HIV protease -log(IC50) M	4311	6274	7.30±1.71
LOGD*	ADME	logD measured by HPLC method	50000	8921	2.70±1.17
METAB*	ADME	percent remaining after 30 min microsomal incubation	2092	4595	23.2±/-33.9
NAV	ADME	Inhibition of Nav1.5 ion channel -log(IC50) M	50000	8302	4.77±0.40
NK1*	Target	Inhibition of neurokinin1 (substance P) receptor binding -log(IC50) M	13482	5803	8.28±1.21
OX1*	Target	Inhibition of orexin 1 receptor -log(Ki) M	7135	4730	6.16±1.22
OX2*	Target	Inhibition of orexin 2 receptor -log(Ki) M	14875	5790	7.25±1.46
PAPP	ADME	Apparent passive permeability in PK1 cells log(permeability) cm/sec	30938	7713	1.35±0.39
PGP*	ADME	Transport by p-glycoprotein log(BA/AB)	8603	5135	0.27±0.53
PPB*	ADME	human plasma protein binding log(bound/unbound)	11622	5470	1.51±0.89
PXR	ADME	Induction of 3A4 by pregnane X receptor; percentage relative to rifampicin	50000	9282	42.5±42.1
RAT_F*	ADME	log(rat bioavailability) at 2mg/kg	7821	5698	1.43±0.76

TDI*	ADME	time dependent 3A4 inhibitions log(IC50 without NADPH/ IC50 with NADPH)	5559	5945	0.37±0.48
THROMBIN*	Target	human thrombin inhibition -log(IC50) M	6924	5552	6.67±2.02

* Kaggle data sets

As an example of qualified data, one might know that the measured $IC_{50} > 30\mu M$ only because $30\mu M$ was the highest concentration titrated, and the assay did not reach an inflection point up to that dose. For the purposes of model-building those activities are treated as fixed numbers, because most off-the-shelf QSAR methods handle only fixed numbers. For example, $IC_{50} > 30\mu M$ is set to $IC_{50}=30 \times 10^{-6} M$ or $-\log(IC_{50})=4.5$. Our experience is that it is best to keep such qualified data in QSAR training sets; otherwise less active compounds are often predicted to be more active than they really are.

In order to compare the predictive ability of QSAR methods, each of these data sets was split into two non-overlapping subsets: a training set and a test set. Our training and test sets are generated by "time-split". For each data set, the first 75% of the molecules assayed form the training set, while the remaining 25% of the compounds assayed later form the test set. We have found that, for regressions, R^2 from time-split validation better estimates the R^2 for true prospective prediction than R^2 from any "split at random" scheme (Sheridan, 2013). Since training and test sets are not selected from the same pool of compounds, the descriptor distributions in these two subsets are frequently not the same.

QSAR Descriptors

Each molecule is represented by a list of features, i.e. "descriptors" in QSAR nomenclature. In this paper, we use a set of descriptors that is the union of AP, the original "atom pair" descriptor from Carhart et al. (1985). and DP descriptors ("Donor acceptor Pair"), called "BP" in Kearsley et al. (1996) Both descriptors are of the form:

Atom type i – (distance in bonds) – Atom type j

For AP, atom type includes the element, number of nonhydrogen neighbors, and number of pi electrons; it is very specific. For DP, atom type is one of seven (cation, anion, neutral donor, neutral acceptor, polar, hydrophobe, and other); it contains a more generic description of chemistry.

Random Forest

RF is an ensemble recursive partitioning method where each recursive partitioning "tree" is generated from a bootstrapped sample of compounds, and a random subset of descriptors is used at the branching of each node in the tree. While there are a few adjustable hyperparameters (e.g. number of trees, fraction of descriptors used at each branching, and size of nodes below which no further splitting should be done), the quality of predictions is generally insensitive to changes in these hyperparameters.

The version of RF we are using is a modification of the original FORTRAN code from Breiman (2001), which is built for regressions. It has been parallelized to run one tree per processor on a cluster. Such parallelization is necessary to run some of our larger data sets in a reasonable time. For all RF models, we generate 100 trees with $m/3$ descriptors used at each branch-point, where m is the number of unique descriptors in the training set. The tree nodes with 5 or fewer molecules are not split further. We apply these hyperparameters to every data set.

Deep Neural Nets

Our Python-based DNN code for fully-connected neural nets is the one obtained through the Kaggle competition from George Dahl (Dahl et al., 2014), then at the U. of Toronto, and modified by us, and deposited in GitHub (<https://github.com/Merck/DeepNeuralNet-QSAR>). The DNN results we present are for single-task regression models using the “standard parameters” in Ma et al. (2015), which are applied to all data sets. For timing purposes, we also have implemented a simplified (“quick”) version of the DNN, which achieves almost identical prediction accuracy to the standard parameters, but uses a smaller neural net. Those parameters are in Sheridan et al. (2016).

XGBoost

The implementation of XGBoost is the C++ version runnable on Linux. <https://picnet.com.au/blog/xgboost-windows-x64-binaries-for-download/>. There are several dozen adjustable hyperparameters of which four we consider “standard” for QSAR problems. These are given in Sheridan et al. (2016). We were able to show that these standard parameters, which are used for all datasets, lead to predictions as good as those where the parameters were optimized for each dataset separately.

Light Gradient Boosting Machine

We are using the Python version downloadable from <https://github.com/microsoft/LightGBM>. The version used for the current study is 2.2.2.

Metrics

In this paper, the metric used to evaluate prediction performance is R^2 , the squared Pearson correlation coefficient between predicted and observed activities in the test set. R^2 is an attractive measurement for model comparison across many data sets because it is unitless and ranges from 0 to 1 for all data sets. The relative predictivity of the three methods we examine does not change if we use alternative metrics such as Q^2 or RMSE.

Workflow for LightGBM hyperparameter optimization

One goal is to identify a set of hyperparameters that would be useful for most QSAR data sets, as was done for other methods. We considered 5 hyperparameters for optimization, the rest were the default.

nrounds, the total number of trees in the model

learnrate, the weight on each tree

nleaves, the maximum number of leaves per tree. An alternative to controlling the complexity of an individual tree is *maxdepth*, which is the maximum depth of a tree. The maximum possible number of leaves per tree is 2^{maxdepth} .

bagfrac, the fraction of compounds randomly selected to create each tree

featfrac, the fraction of descriptors randomly selected to create each tree

We follow a similar workflow for hyperparameter optimization as we did with XGBoost (Sheridan et al., 2016). Whereas for XGBoost we optimized three hyperparameters in a full grid search, for five hyperparameters a step-wise grid search was more practical. For each dataset the hyperparameters were optimized in the following way.

1. An “original” set of hyperparameter was *nrounds*=1500, *learnrate*=0.01, *nleaves*=32, *bagfrac*=0.7, *featfrac*=0.7.
2. A grid search was done on *nrounds*=(1500,700,350,100) and *learnrate*=(0.01,0.02,0.05,0.1). Other hyperparameters as in the original.
3. Given the optimum combination of *nrounds* and *learnrate*, a grid search was done on *nleaves*=(16,32,64,128,256).
4. Given the optimum combination of *nrounds*, *learnrate*, and *nleaves*, a grid search was done for *featfrac*=(0.25,0.50,0.7,1.0) and *bagfrac*=(0.25,0.50,0.7,1.0)

Searches were done under two different circumstances.

1. TESTOPT: Find the optimum combination of hyperparameters that gives the highest average R^2 for the test sets. It should be noted that TESTOPT does not reflect a realistic situation, because we would not know the activity values of the test set in advance. However, this gives us an upper limit for the R^2 on the test set we can expect by optimizing these hyperparameters, and it is interesting to know what hyperparameter values we should use *if* we had prior knowledge. TESTOPT finds a different set of optimum hyperparameters for each data set.

2. TRAINOPT: Finding the optimal values by cross-validation of each training set. That is, split the training set in half randomly, make a model from the first half using the hyperparameters, and then predict the remaining half. The set of hyperparameters that gives the highest R^2 for the prediction of the second half of the training set is used to generate a model using the entire training set. This model is used to predict the test set. This is more realistic situation because we are optimizing only on the training set. TRAINOPT finds a different set of hyperparameters for each data set.

3. STANDARD. The goal is to find a common value of *nrounds*, *learnrate*, *nleaves*, *bagfrac*, and *featfrac* to be used for all data sets. The most straightforward way of generating such a standard set is to find the mean optimum values of the five hyperparameters in TESTOPT, TRAINOPT, or both.

Assessing Uncertainty of Predictions

A way to assess uncertainty of prediction is with prediction intervals: A 95% prediction interval (L,U) for a molecule indicates that with 95% probability the prediction on the model derived from the actual data should be larger than L and smaller than U. One typical method of generating these intervals is via quantile regression. For RF, the algorithm can be exploited to generate such intervals with some manipulation of output (Meinshausen, 2006). When predicting the activity of a molecule, for each tree in the forest, the molecule will end up in a terminal node. The molecules in the training set that also landed in that terminal nodes are considered neighbors of the molecules being predicted. Aggregating these neighbors across all trees in the forest, we can form prediction intervals by computing the weighted 2.5th and 97.5th weighted percentiles of the activities of these neighbors, the weights being the frequency that a molecule appears as a neighbor over all trees. BART, being a Bayesian method, naturally outputs a distribution for each point being predicted, and the quantiles of the distribution (e.g., 2.5th and 97.5th percentiles) serve as the prediction interval. LightGBM provides the option of the quantile loss function that can be used to predict the given quantile. To generate prediction intervals, one would build two LightGBM models, one for the lower limit (e.g., the 2.5th percentile) and another for the upper limits (e.g., 97.5th percentile).

Timing

The three methods we are comparing RF, DNN, and XGBoost/LightGBM work on different machine architectures and/or modes in our environment:

1. RF runs as 100 jobs (one for each tree) running in parallel on a cluster. The cluster nodes are HP ProLiant BL460c Gen8 server blades, each equipped with two 8 core Intel(R) Xeon(R) CPU E5-2670 0 @ 2.60GHz processors and 256GB Random Access Memory (RAM). The total time is the time for a single job times 100.
2. XGBoost and LightGBM run on a single node of the above cluster.
3. DNN runs on a single NVIDIA Tesla C2070 GPU . The GPU runs almost exactly 10-fold faster than the cluster nodes, so the total time for a DNN on a cluster node would be 10 times the time for running on the GPU.

Model size

Another interesting aspect of a QSAR method is the size of the model file, in that the speed of prediction is sometimes limited in practice by the time taken to read the model into memory or by copying the model from an archive to the computer doing the predicting. Here we note the size of the (binary) files comprising the model. In the case of RF, we multiply the size of a single tree by 100. In practice the size of a model file can vary depending on the particular implementation of the QSAR method, including compression of the file, but looking at the size will give us a rough idea of the relative complexity of models from the respective methods.

RESULTS

Optimizations and standard hyperparameters for LightGBM

The optimum set of hyperparameters for individual data sets and the R^2 for each type of optimization are in Supporting Information. As with XGBoost, we find that the prediction accuracy is not particularly sensitive to the hyperparameters we examined. Mean optimum hyperparameter values are shown in Table 2. While the optimum values of hyperparameters do not correlate well between TESTOPT and TRAINOPT for individual data sets (not shown), the mean optimum hyperparameter values for TESTOPT and TRAINOPT are not far apart relative to the overall range of each hyperparameter. We averaged over both TESTOPT and TRAINOPT for all datasets to obtain the standard hyperparameters. It is interesting that the STANDARD value of *bagfrac* is close to the fraction of compounds that would appear through bagging in random forest (0.66), and the STANDARD value of *featfrac* is close to the descriptors/3 (0.33) rule for regressions in random forest. Predictions using these values are called LightGBM_STANDARD. An independent study from our laboratory (DiFranzo et al., 2020) used the same datasets, but built models using only compounds similar to those in the test set. The hyperparameters for LightGBM, generated by a more automated procedure, are also listed in Table 2. They are not dissimilar.

Table 2. Mean optimal values for five hyperparameters averaged over 30 datasets

Hyperparameter	TESTOPT	TRAINOPT	STANDARD	DiFranzo et al.
<i>nrounds</i>	1089 \pm 550	1306 \pm 342	1200	1000
<i>learnrate</i>	0.027 \pm 0.019	0.029 \pm 0.02	0.028	0.05
<i>nleaves</i>	84 \pm 77	58 \pm 51	72	\leq 128 (<i>maxdepth</i> =7)
<i>bagfrac</i>	0.68 \pm 0.24	0.73 \pm 0.26	0.71	0.5
<i>featfrac</i>	0.45 \pm 0.25	0.35 \pm 0.19	0.40	0.2

In TRAINOPT there is a relationship between the optimum *learnrate*, *nleaves* and *bagfrac* vs. Ntraining, the number of molecules in the training set: smaller data sets tend to prefer smaller values of these hyperparameters. Therefore, it might be possible to guess a good value for these hyperparameters for individual data sets based only on Ntraining. However, we will show below that the STANDARD hyperparameters already give almost as good predictions as the TRAINOPT grid-search, so this type of refinement is not likely to be helpful overall. We made similar observations with XGBoost.

Accuracy of prediction for the QSAR methods

Figure 1 (Top) shows the R^2 for prediction of the test set for DNN_STANDARD, XGBOOST_STANDARD, LightGBM_TRAINOPT and LightGBM_STANDARD vs. the R^2 for RF, which we are taking as the baseline method. Figure 1 (Bottom) shows the R^2 for prediction minus the R^2 for RF vs. the R^2 for RF, which better shows small differences between methods. Generally speaking, LightGBM_TRAINOPT might be more predictive than LightGBM_STANDARD, indicating there

might theoretically be a reason to optimize the hyperparameters for individual datasets, but this difference is very small; both are generally at least as good as DNN in predictivity. Thus, in our opinion, the much greater time to optimize QSAR datasets would not be justified, and STANDARD hyperparameters could be used to good effect. The overall predictivity of LightGBM_STANDARD hyperparameters is very close to that of the original hyperparameters, supporting the idea that a range of hyperparameter values is acceptable.

The visual impression in Figure 1 is consistent with the mean R^2 over the 30 data sets as shown in Table 3. Although representing an unrealistic scenario, one would expect LightGBM_TESTOPT set results to get slightly higher predictivity than LightGBM_TRAINOPT, and it does. These are only averages; any of the four methods may do best on a particular data set.

Table 3. Mean R^2 for 30 datasets for methods using the AP,DP descriptor:

Method	Mean R^2
RF	0.39
DNN STANDARD	0.43
XGBoost STANDARD	0.43
LightGBM TRAINOPT	0.45
LightGBM STANDARD	0.44
LightGBM TESTOPT	0.46

Timing

Total compute time is shown in Figure 2 as a function of N_{training} . The log-log plot is the one where all methods show a maximally linear correlations and the range of timings can be appreciated. The total compute effort for DNN, XGBoost, and LightGBM using standard hyperparameters are roughly linear with N_{training} . As expected, the DNN using fewer neurons (“quick”) requires less computation than the standard DNN. The total compute effort for RF rises roughly as the square of N_{training} . Clearly, boosting methods are much faster than RF and DNN in total compute effort, at least for the larger data sets, and LightGBM is faster than XGBoost by a factor of almost 4.

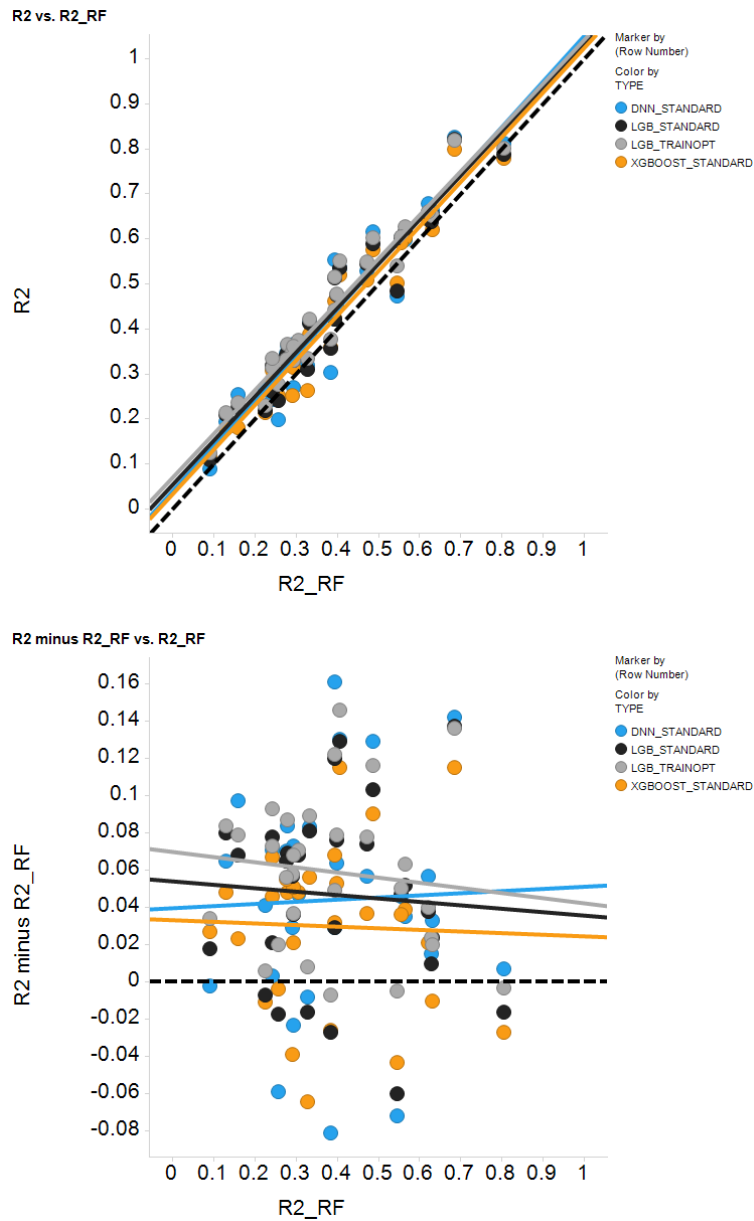


Figure 1. Prediction accuracy on the test set for DNN, XGBoost, and LightGBM and deep neural nets vs. the prediction accuracy of random forest. Two different types of LightGBM hyperparameters are shown, one with the hyperparameters optimized for individual training sets (grey), and one using a standard set of hyperparameters for all data sets (black). (Top) The absolute R^2 . (Bottom) The R^2 minus the R^2 for random forest.

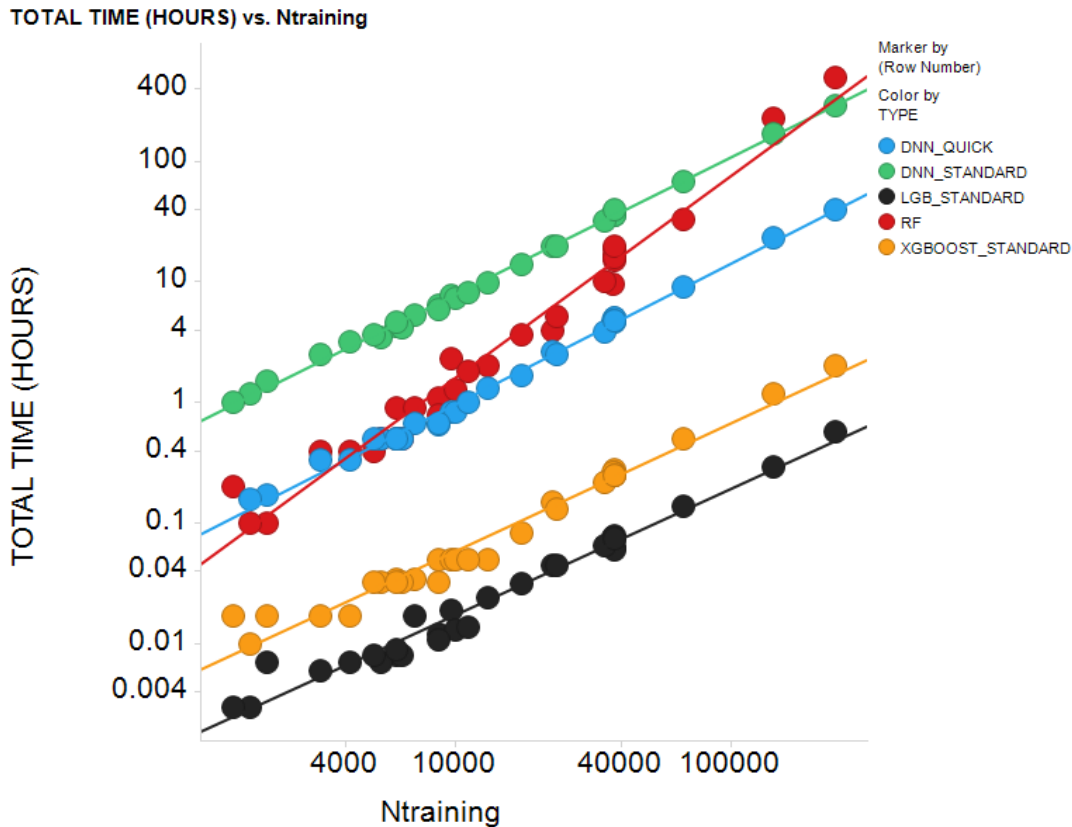


Figure 2. Total computational effort (Top) for random forest, deep neural nets, XGBoost, and LightGBM. The computational effort is expressed in units of hours on a single cluster node.

Model size

Total model file size (in megabytes) is shown in Figure 3 as a function of Ntraining. The log-log plot is the one where all methods show a maximally linear correlations and the range of model file sizes can be appreciated. The size of DNN models is expected to depend on the total number of neurons. The number of neurons of the lowest layer will depend on the number of descriptors, which varies roughly as $\log(N_{\text{training}})$, and the number of neurons in the intermediate layers will depend on the number of intermediate layers and number of neurons per layer set by the user. Effectively, the dependence of size is approximately $\log(N_{\text{training}})$. We would expect networks with fewer layers and fewer neurons per layer (the “quick” DNN) to produce smaller models than the original standard DNN, and they do. In contrast, the number of nodes in an unpruned recursive partitioning tree should be linear with Ntraining, and we see this for RF. There is a small dependence of size of XGBoost models roughly with $\log(N_{\text{training}})$, which probably reflects the fact that larger data sets have more trees closer to the maximum depth. The model size of LightGBM_STANDARD is constant for all models, at ~ 7 megabytes, somewhat bigger than for XGBoost. LightGBM models using the original hyperparameters (not shown in the figures) are ~ 4 megabytes, probably reflecting the smaller value of *nleaves* (32 vs. 72). Both flavors of boosting generate models that are tiny compared to those from RF and DNN.

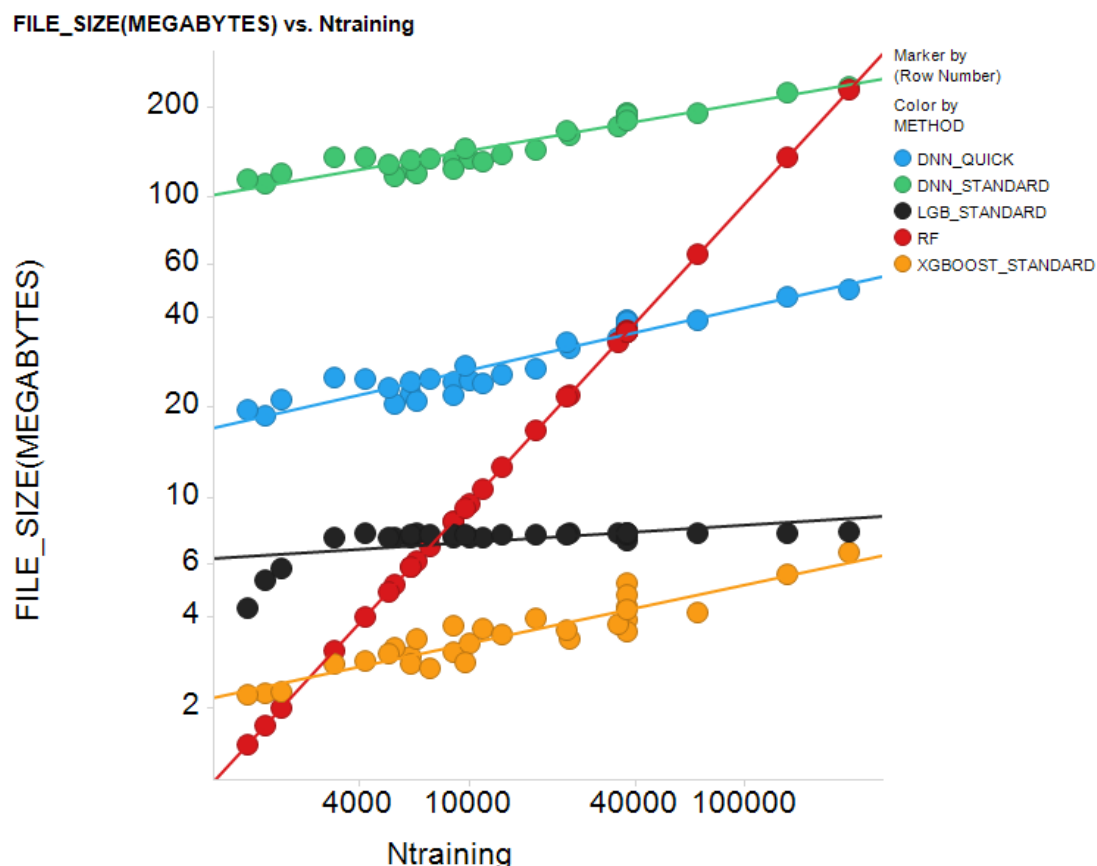
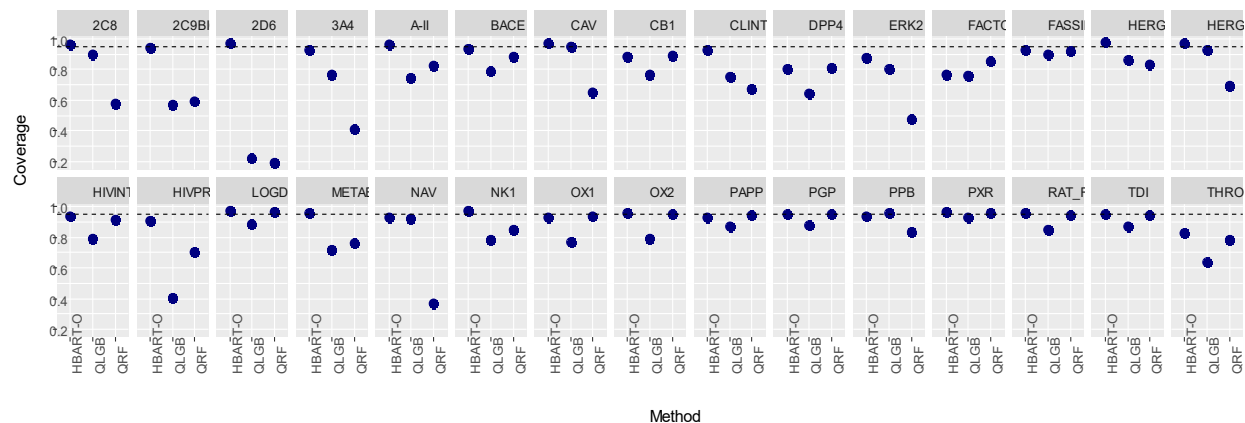


Figure 3. Total model file size for the QSAR methods.

Uncertainty of Prediction

For assessing prediction uncertainty with prediction intervals, we evaluate three methods: BART, quantile regression forest (QRF), and quantile regression using LightGBM (QLGB), by comparing the coverage on the test set data. Coverage is the fraction of the data point for which the observed activity falls within the prediction intervals. Since we generated 95% prediction intervals, we expect to see approximately 95% of the data to fall within (“covered by”) the intervals. Figure 4A shows the comparison of the coverage of the three methods on the 30 datasets. Quantile regression using LightGBM gives good coverage for most of the datasets. It does better than quantile regression forests but not as well as BART. Figure 4B shows the median widths of the prediction intervals, normalized to the minimum median width across methods within each data set. For methods with comparable coverages, one naturally prefers methods with smaller prediction intervals (indicating less uncertainty). Even though lightGBM tend to have shorter interval widths compared to BART and RF, one should take into account the coverages are not necessarily comparable.



B

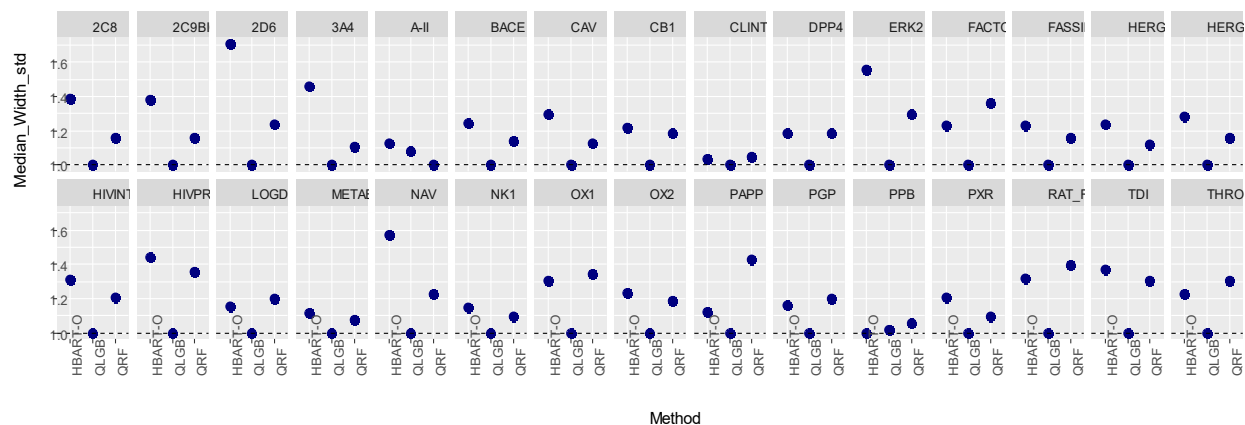


Figure 4. Coverage (A) and median width (B) of the error estimation of BART, Quantile Random Forest, and LightGBM.

DISCUSSION

Most of the current attention in QSAR is on various deep neural net architectures, and these seem to have an edge over more traditional methods in terms of accuracy in prediction. This is especially true of neural net methods that do not use explicit input descriptors, but use "convolution" on individual atomic or bond properties to effectively generate their own problem-specific descriptor types on-the-fly (Feinberg, et al. 2020; Chuang et al., 2020; Walters and Barzilay, 2021). However, under many circumstances computational efficiency is at least as important as accuracy. Boosting appears to be a very effective and efficient class of machine-learning methods. Previously we showed that XGBoost achieves predictions for QSAR datasets as good as that from single-task DNN and it does it for orders of magnitude less total compute time and produces much smaller models. Here we demonstrated that LightGBM, tested on diverse QSAR problems, produces slightly better predictions than XGBoost, and takes even less compute time. This is consistent with the observations of Zhang et al. (2019) on toxicity problems using random-split validation. Having LightGBM means we can potentially handle

many more and larger data sets and/or update them more frequently than we have previously, given our current compute environment.

The potential difficulty LightGBM having multiple adjustable hyperparameters turns out, in practice, to not be a real issue for QSAR because we can identify standard values of at least some hyperparameters. As we have previously showed with DNN and XGBoost, standard hyperparameters can be used effectively with a large number of QSAR data sets, so that it is not necessary to optimize the hyperparameters for each individual data set. As well as taking a great deal of time, optimization has the additional drawback that it might not be as effective as hoped in true prospective prediction. It is a tacit assumption in QSAR that the molecules to be predicted (in the test set) are similar enough to the training set that maximizing the cross-validated predictions of the training set (by using different descriptors, tweaking adjustable hyperparameters, etc.) is equivalent to maximizing predictivity on the test set. In practice, the training and test sets may be different enough that this is not true. The fact that the optimum hyperparameters in LightGBM_TRAINOPT and LightGBM_TESTOPT do not correlate, and that similar findings were made for XGBoost (Sheridan et al., 2016) and DNN (Ma et al., 2015), supports this.

Recursive partitioning methods like RF, XGBoost, and LightGBM make predictions based on the average observed activities of molecules at their terminal nodes. This has the effect of compressing the range of predictions relative to the observed activities. For random forest we routinely do “prediction rescaling” (Sheridan, 2014), where the self-fit predicted activities in the training set of a particular model are linearly scaled to match the observed activities, and this scaling is applied to further predictions from that model. This does not affect the R^2 of prediction, but does help the numerical match of predicted and observed activities at the highest and lowest ranges of activity. We have found XGBoost and LightGBM also benefit from prediction rescaling.

LightGBM also provides a way to assess uncertainty of predictions via quantile regression, something not available in XGBoost. It does entail having to build a separate model for each end of the interval (i.e., one model for the lower limit and another for the upper limit), but the efficiency of the software is such that building extra models with LightGBM can still take less time than with other methods. While LightGBM uncertainties are perhaps not as good in terms of coverage as those in BART (this paper) or as good as Gaussian Processes (DiFranzo et al., 2020), they are somewhat better than those from Quantile RF (this paper). A detailed comparison of the lightGBM intervals to a wider variety of methods will be published elsewhere.

ACKNOWLEDGEMENTS

We thank Dai Feng for generating the results for BART and quantile random forests in Figure 4.

CONFLICT OF INTEREST

The authors declare no financial conflict of interest.

REFERENCES

- Anghel, A.; Papandreou, N.; Parnell, T.; De Palma, A.; Pozidis, H. Benchmarking and Optimization of Gradient Boosting Decision Tree Algorithms arXiv:1809.04559v3 (2019)
- Breiman, L. Random Forests. *Machine Learning* **2001**, 45, 3-32.
- Carhart, R. E.; Smith, D. H.; Ventkataraghavan, R. Atom Pairs as Molecular Features in Structure-Activity Studies: Definition and Application. *J. Chem. Inf. Comput. Sci.*, **1985**, 25, 64-73.
- Chen, T.; Guestrin, C. XGBoost: A Scalable Tree Boosting System. arXiv:1603.02754v3 2016
- Chuang, K.V.; Gunsalus, L.M.; Keiser, M.J. Learning Molecular Representations for Medicinal Chemistry, *J. Med. Chem.*; **2020**, 63, 8705-8722.
- Dahl, G.E.; Jaitly, N.; Salakhutdinov, R. Multi-Task Neural Networks for QSAR Predictions. **2014**, arXiv:1406.1231 [stat.ML]. <http://arxiv.org/abs/1406.1231>
- DiFranzo, A.; Sheridan, R.P.; Liaw, A.; Tudor, M. Nearest Neighbor Gaussian Process for Quantitative Structure-Activity Relationships. *J. Chem. Inf. Model.* **2020**, 60, 4053-4663.
- Du, G.; Ma, L.; Hu, J.-S.; Zhang, J.; Xiang, Y.; Shao, D.; Wang, H. Prediction of 30-Day Readmission: An Improved Gradient Boosting Decision Tree Approach *Journal of Medical Imaging and Health Informatics*. **2019**, 9, 620-627.
- Feinberg, E.N.; Joshi, E.; Pande, V.S.; Cheng, A.C. Improvement in ADMET Prediction with Multitask Deep Featurization. *J. Med. Chem.* **2020**, 63, 8835-8848.
- Feng, D.; Svetnik, V.; Liaw, A.; Pratola, M.; Sheridan, R.P. Building Quantitative Structure-Activity Relationship Models Using Bayesian Additive Regression Trees. *J. Chem. Inf. and Model.* **2019**, 59, 2642-2655.
- Friedman, J. Greedy Function Approximation: a Gradient Boosting Machine. *Annals of Statistics* 2001, **29**, 1189-1232.
- Gawehn, E.; Hiss, J.A.; Schneider, G. Deep Learning in Drug Discovery. *Mol. Inf.* **2016**, 35, 3-14.
- Ke, G.; Meng, Q.; Finley, T.; Wang, T.; Chen, W.; Ma, Weidong, Ye, Q.; Liu, T.-Y. LightGBM: A Highly Efficient Gradient Boosting Decision Tree 31st Conference on Neural Information Processing Systems (NIPS 2017), Long Beach, CA, USA.
- Kearsley, S.K.; Sallamack, S.; Fluder, E.M.; Andose, J.D.; Mosley, R.T.; Sheridan, R.P. Chemical Similarity Using Physicochemical Property Descriptors. *J. Chem. Inform. Comp. Sci.* **1996**, 36, 118-27.

Ma, J.; Sheridan, R.P.; Liaw, A.; Dahl, G.E.; Svetnik, V. Deep Neural Nets as a Method for Quantitative-Structure-Activity Relationships. *J. Chem. Inf. Model.* **2015**, *55*, 263-274.
Meinshausen, N. Quantile Regression Forests. *J. Machine Learning Res.* 2006, *7*, 983-999.

Omar, K.B.A. XGBoost and LGBM for Porto Seguro's Kaggle Challenge: A Comparison. *Distributed Computing* <https://pub.tik.ee.ethz.ch/students/2017-HS/SA-2017-98.pdf>

Sheridan, R.P. Time-Split Cross-Validation as a Method For Estimating the Goodness of Prospective Prediction. *J. Chem. Inf. Model.* **2013**, *53*, 783-790.

Sheridan, R.P. Global Quantitative Structure-Activity Relationship Models vs. Selected Local Models as Predictors of Off-Target Activities for Project Compounds. *J. Chem. Inf. Model.* **2014**, *54*, 1083-1092.

Sheridan, R.P.; Wang, W.M.; Liaw, A.; Ma, J.; Gifford, E.M. Extreme Gradient Boosting as a Method for Quantitative-Structure Activity Relationships. *J. Chem. Inf. Model.* **2016**, *56*, 2353-2360.

Sheridan, R.P.; Wang, M.; Liaw, A.; Ma, J.; Gifford, E. Correction to Extreme Gradient Boosting as a Method for Quantitative Structure-Activity Relationships. *J. Chem. Inf. Model.* **2020**, *60*, 1910.

Svetnik, V.; Liaw, A.; Tong, C.; Culberson, J.C.; Sheridan, R.P.; Feuston, B.P. Random Forest: A Classification and Regression Tool for Compound Classification and QSAR Modeling. *J. Chem. Inf. Comput. Sci.* **2003**, *43*, 1947-1958.

Walters, W.P.; Barzilay, R. Applications of Deep Learning in Molecular Generation and Property Prediction. *Acc. Chem. Res.* **2021**, *54*, 263-270.

Zhang, J.; Mucs, D.; Norinder, U.; Svensson, F. LightGBM: An Effective and Scalable Algorithm for Prediction of Chemical Toxicity—Application to the Tox21 and Mutagenic Data Sets. *J. Chem. Inf. Model.* **2019**, *59*, 4150-4158.

SUPPORTING INFORMATION

1. Hyperparameters for TESTOPT TRAINOPT of LightGBM.

Data set	nrounds_ TESTOPT	learnrate_ TESTOPT	nleaves_ TESTOPT	featfrac_ TESTOPT	bagfrac_ TESTOPT	nrounds_T RAINOPT	learnrate_ TRAINOPT	nleaves_T RAINOPT	featfrac_T RAINOPT	bagfrac_T RAINOPT
2C8	700	0.1	256	0.7	0.25	1500	0.02	64	0.7	0.25
2C9BI G	1500	0.05	256	0.5	0.25	1500	0.1	256	0.7	1
2D6	1500	0.02	128	1	0.5	1500	0.02	64	1	0.5
3A4	1500	0.05	128	0.7	0.5	1500	0.05	64	0.7	0.5
ANRIN A	700	0.02	32	1	0.7	700	0.01	16	1	0.25
BACE	1500	0.01	32	0.5	0.5	1500	0.02	32	1	0.25
CAV	1500	0.02	32	0.7	0.25	1500	0.05	128	1	0.25
CB1	1500	0.01	64	0.5	0.7	700	0.01	16	0.25	0.25
CLINT	1500	0.02	128	0.5	0.5	1500	0.02	64	1	0.25
DPP4	350	0.01	256	0.25	0.5	1500	0.01	16	0.25	0.25
ERK2	700	0.02	16	1	0.25	1500	0.01	16	0.7	0.25
FACT ORXIA	100	0.01	16	1	1	1500	0.01	32	0.7	0.25
FASSIF	1500	0.02	128	0.5	1	1500	0.05	128	1	0.7
HIV_I NT	100	0.01	16	0.25	1	700	0.02	16	1	0.25
HIV_P ROT	100	0.02	16	1	0.7	700	0.01	16	0.25	0.25
HPLC_ LOGD	1500	0.05	64	0.7	0.5	1500	0.05	64	1	0.25
META B	1500	0.01	64	0.7	0.25	1500	0.05	64	1	0.5
MK49 9	1500	0.02	128	0.7	0.25	1500	0.05	128	0.7	0.5
NAV	1500	0.02	256	1	0.25	1500	0.05	64	1	0.5
NK1	700	0.02	32	1	0.25	700	0.02	16	0.25	0.25
OX1	1500	0.05	32	0.5	0.25	1500	0.01	32	1	0.25
OX2	1500	0.01	32	0.5	0.25	1500	0.02	32	0.7	0.25
PAPP	1500	0.05	64	1	0.25	1500	0.05	64	0.7	0.25
PGP	700	0.05	64	0.5	0.25	1500	0.02	32	0.7	0.25
PPB	1500	0.02	32	0.7	0.5	1500	0.02	32	0.5	0.25
PXR	1500	0.02	64	0.7	0.25	1500	0.05	128	0.7	0.25
RAT_F	350	0.02	32	0.7	0.25	700	0.02	32	0.7	0.5
TDI	100	0.02	64	0.7	0.7	700	0.01	64	0.5	0.7
THRO MBIN	1500	0.02	32	0.25	0.25	1500	0.01	32	0.5	0.25

2. R² for STANDARD methods

DATASET	R2	TYPE
2C8	0.158	RF
2C9BIG	0.279	RF
2D6	0.13	RF
3A4	0.471	RF
A-II	0.805	RF
BACE	0.629	RF
CAV	0.399	RF
CB1	0.292	RF
CLINT	0.393	RF
DPP4	0.225	RF
ERK2	0.257	RF
FACTORXIA	0.241	RF
FASSIF	0.294	RF
HERG	0.305	RF
HERGBIG	0.294	RF
HIV_INT	0.327	RF
HIV_PROT	0.545	RF
HPLC_LOGD	0.684	RF
METAB	0.631	RF
NAV	0.277	RF
NK1	0.393	RF
OX1	0.487	RF
OX2	0.564	RF
PAPP	0.621	RF
PGP	0.556	RF
PPB	0.406	RF
PXR	0.333	RF
RAT_F	0.091	RF
TDI	0.385	RF
THROMBIN	0.242	RF
2C8	0.255	DNN_STANDARD
2C9BIG	0.363	DNN_STANDARD
2D6	0.195	DNN_STANDARD
3A4	0.528	DNN_STANDARD
A-II	0.812	DNN_STANDARD
BACE	0.644	DNN_STANDARD
CAV	0.463	DNN_STANDARD
CB1	0.321	DNN_STANDARD
CLINT	0.554	DNN_STANDARD
DPP4	0.266	DNN_STANDARD
ERK2	0.198	DNN_STANDARD
FACTORXIA	0.244	DNN_STANDARD
FASSIF	0.271	DNN_STANDARD
HERG	0.352	DNN_STANDARD
HERGBIG	0.367	DNN_STANDARD
HIV_INT	0.319	DNN_STANDARD
HIV_PROT	0.473	DNN_STANDARD
HPLC_LOGD	0.826	DNN_STANDARD
METAB	0.664	DNN_STANDARD
NAV	0.347	DNN_STANDARD
NK1	0.422	DNN_STANDARD
OX1	0.616	DNN_STANDARD

OX2	0.599	DNN_STANDARD
PAPP	0.678	DNN_STANDARD
PGP	0.602	DNN_STANDARD
PPB	0.536	DNN_STANDARD
PXR	0.416	DNN_STANDARD
RAT_F	0.089	DNN_STANDARD
TDI	0.304	DNN_STANDARD
THROMBIN	0.313	DNN_STANDARD
2C8	0.207	XGBOOST_TESTOPT
2C9BIG	0.344	XGBOOST_TESTOPT
2D6	0.19	XGBOOST_TESTOPT
3A4	0.517	XGBOOST_TESTOPT
A-II	0.802	XGBOOST_TESTOPT
BACE	0.656	XGBOOST_TESTOPT
CAV	0.459	XGBOOST_TESTOPT
CB1	0.281	XGBOOST_TESTOPT
CLINT	0.474	XGBOOST_TESTOPT
DPP4	0.23	XGBOOST_TESTOPT
ERK2	0.287	XGBOOST_TESTOPT
FACTORXIA	0.386	XGBOOST_TESTOPT
FASSIF	0.318	XGBOOST_TESTOPT
HERG	0.355	XGBOOST_TESTOPT
HERGBIG	0.36	XGBOOST_TESTOPT
HIV_INT	0.298	XGBOOST_TESTOPT
HIV_PROT	0.587	XGBOOST_TESTOPT
HPLC_LOGD	0.804	XGBOOST_TESTOPT
METAB	0.625	XGBOOST_TESTOPT
NAV	0.33	XGBOOST_TESTOPT
NK1	0.435	XGBOOST_TESTOPT
OX1	0.578	XGBOOST_TESTOPT
OX2	0.612	XGBOOST_TESTOPT
PAPP	0.646	XGBOOST_TESTOPT
PGP	0.606	XGBOOST_TESTOPT
PPB	0.538	XGBOOST_TESTOPT
PXR	0.391	XGBOOST_TESTOPT
RAT_F	0.125	XGBOOST_TESTOPT
TDI	0.38	XGBOOST_TESTOPT
THROMBIN	0.342	XGBOOST_TESTOPT
2C8	0.202	XGBOOST_TRAINOPT
2C9BIG	0.344	XGBOOST_TRAINOPT
2D6	0.187	XGBOOST_TRAINOPT
3A4	0.515	XGBOOST_TRAINOPT
A-II	0.769	XGBOOST_TRAINOPT
BACE	0.651	XGBOOST_TRAINOPT
CAV	0.45	XGBOOST_TRAINOPT
CB1	0.225	XGBOOST_TRAINOPT
CLINT	0.458	XGBOOST_TRAINOPT
DPP4	0.218	XGBOOST_TRAINOPT
ERK2	0.266	XGBOOST_TRAINOPT
FACTORXIA	0.271	XGBOOST_TRAINOPT
FASSIF	0.314	XGBOOST_TRAINOPT
HERG	0.352	XGBOOST_TRAINOPT
HERGBIG	0.355	XGBOOST_TRAINOPT
HIV_INT	0.273	XGBOOST_TRAINOPT
HIV_PROT	0.551	XGBOOST_TRAINOPT
HPLC_LOGD	0.804	XGBOOST_TRAINOPT

METAB	0.611	XGBOOST_TRAINOPT
NAV	0.328	XGBOOST_TRAINOPT
NK1	0.433	XGBOOST_TRAINOPT
OX1	0.553	XGBOOST_TRAINOPT
OX2	0.589	XGBOOST_TRAINOPT
PAPP	0.639	XGBOOST_TRAINOPT
PGP	0.606	XGBOOST_TRAINOPT
PPB	0.526	XGBOOST_TRAINOPT
PXR	0.387	XGBOOST_TRAINOPT
RAT_F	0.103	XGBOOST_TRAINOPT
TDI	0.356	XGBOOST_TRAINOPT
THROMBIN	0.342	XGBOOST_TRAINOPT
2C8	0.181	XGBOOST_STANDARD
2C9BIG	0.327	XGBOOST_STANDARD
2D6	0.178	XGBOOST_STANDARD
3A4	0.508	XGBOOST_STANDARD
A-II	0.778	XGBOOST_STANDARD
BACE	0.651	XGBOOST_STANDARD
CAV	0.452	XGBOOST_STANDARD
CB1	0.253	XGBOOST_STANDARD
CLINT	0.461	XGBOOST_STANDARD
DPP4	0.214	XGBOOST_STANDARD
ERK2	0.253	XGBOOST_STANDARD
FACTORXIA	0.308	XGBOOST_STANDARD
FASSIF	0.315	XGBOOST_STANDARD
HERG	0.353	XGBOOST_STANDARD
HERGBIG	0.345	XGBOOST_STANDARD
HIV_INT	0.263	XGBOOST_STANDARD
HIV_PROT	0.502	XGBOOST_STANDARD
HPLC_LOGD	0.799	XGBOOST_STANDARD
METAB	0.621	XGBOOST_STANDARD
NAV	0.332	XGBOOST_STANDARD
NK1	0.425	XGBOOST_STANDARD
OX1	0.577	XGBOOST_STANDARD
OX2	0.603	XGBOOST_STANDARD
PAPP	0.642	XGBOOST_STANDARD
PGP	0.592	XGBOOST_STANDARD
PPB	0.521	XGBOOST_STANDARD
PXR	0.389	XGBOOST_STANDARD
RAT_F	0.118	XGBOOST_STANDARD
TDI	0.359	XGBOOST_STANDARD
THROMBIN	0.288	XGBOOST_STANDARD
2C8	0.189	LGB_ORIGINAL
2C9BIG	0.304	LGB_ORIGINAL
2D6	0.202	LGB_ORIGINAL
3A4	0.521	LGB_ORIGINAL
A-II	0.797	LGB_ORIGINAL
BACE	0.657	LGB_ORIGINAL
CAV	0.471	LGB_ORIGINAL
CB1	0.351	LGB_ORIGINAL
CLINT	0.481	LGB_ORIGINAL
DPP4	0.216	LGB_ORIGINAL
ERK2	0.27	LGB_ORIGINAL
FACTORXIA	0.314	LGB_ORIGINAL
FASSIF	0.318	LGB_ORIGINAL
HERG	0.36	LGB_ORIGINAL

HERGBIG	0.32	LGB_ORIGINAL
HIV_INT	0.339	LGB_ORIGINAL
HIV_PROT	0.52	LGB_ORIGINAL
HPLC_LOGD	0.794	LGB_ORIGINAL
METAB	0.662	LGB_ORIGINAL
NAV	0.314	LGB_ORIGINAL
NK1	0.435	LGB_ORIGINAL
OX1	0.578	LGB_ORIGINAL
OX2	0.614	LGB_ORIGINAL
PAPP	0.65	LGB_ORIGINAL
PGP	0.606	LGB_ORIGINAL
PPB	0.541	LGB_ORIGINAL
PXR	0.394	LGB_ORIGINAL
RAT_F	0.123	LGB_ORIGINAL
TDI	0.365	LGB_ORIGINAL
THROMBIN	0.321	LGB_ORIGINAL
2C8	0.226	LGB_STANDARD
2C9BIG	0.348	LGB_STANDARD
2D6	0.21	LGB_STANDARD
3A4	0.545	LGB_STANDARD
A-II	0.789	LGB_STANDARD
BACE	0.639	LGB_STANDARD
CAV	0.475	LGB_STANDARD
CB1	0.349	LGB_STANDARD
CLINT	0.513	LGB_STANDARD
DPP4	0.218	LGB_STANDARD
ERK2	0.24	LGB_STANDARD
FACTORXIA	0.262	LGB_STANDARD
FASSIF	0.33	LGB_STANDARD
HERG	0.373	LGB_STANDARD
HERGBIG	0.362	LGB_STANDARD
HIV_INT	0.311	LGB_STANDARD
HIV_PROT	0.485	LGB_STANDARD
HPLC_LOGD	0.821	LGB_STANDARD
METAB	0.655	LGB_STANDARD
NAV	0.342	LGB_STANDARD
NK1	0.422	LGB_STANDARD
OX1	0.59	LGB_STANDARD
OX2	0.616	LGB_STANDARD
PAPP	0.659	LGB_STANDARD
PGP	0.603	LGB_STANDARD
PPB	0.535	LGB_STANDARD
PXR	0.414	LGB_STANDARD
RAT_F	0.109	LGB_STANDARD
TDI	0.358	LGB_STANDARD
THROMBIN	0.32	LGB_STANDARD
2C8	0.237	LGB_TRAINOPT
2C9BIG	0.366	LGB_TRAINOPT
2D6	0.214	LGB_TRAINOPT
3A4	0.549	LGB_TRAINOPT
A-II	0.802	LGB_TRAINOPT
BACE	0.653	LGB_TRAINOPT
CAV	0.478	LGB_TRAINOPT
CB1	0.35	LGB_TRAINOPT
CLINT	0.515	LGB_TRAINOPT
DPP4	0.231	LGB_TRAINOPT

ERK2	0.277	LGB_TRAINOPT
FACTORXIA	0.314	LGB_TRAINOPT
FASSIF	0.331	LGB_TRAINOPT
HERG	0.376	LGB_TRAINOPT
HERGBIG	0.362	LGB_TRAINOPT
HIV_INT	0.335	LGB_TRAINOPT
HIV_PROT	0.54	LGB_TRAINOPT
HPLC_LOGD	0.82	LGB_TRAINOPT
METAB	0.651	LGB_TRAINOPT
NAV	0.333	LGB_TRAINOPT
NK1	0.442	LGB_TRAINOPT
OX1	0.603	LGB_TRAINOPT
OX2	0.627	LGB_TRAINOPT
PAPP	0.661	LGB_TRAINOPT
PGP	0.606	LGB_TRAINOPT
PPB	0.552	LGB_TRAINOPT
PXR	0.422	LGB_TRAINOPT
RAT_F	0.125	LGB_TRAINOPT
TDI	0.378	LGB_TRAINOPT
THROMBIN	0.335	LGB_TRAINOPT

3. Timing for all methods

Data set	Ntraining	TYPE	TOTAL TIME (HOURS)
2C8	22500	RF	4
2C9BIG	142000	RF	224
2D6	37500	RF	19
3A4	37499	RF	15
A-II	2072	RF	0.1
BACE	13101	RF	2
CAV	37500	RF	17
CB1	8730	RF	1.1
CLINT	17469	RF	3.7
DPP4	6150	RF	0.9
ERK2	9632	RF	2.3
FACTORXIA	7149	RF	0.9
FASSIF	67100	RF	33.3
HERG	37473	RF	9.6
HERGBIG	238000	RF	494
HIV_INT	1815	RF	0.1
HIV_PROT	3233	RF	0.4
HPLC_LOGD	37500	RF	16
METAB	1569	RF	0.2
NAV	34682	RF	10.1
NK1	10050	RF	1.3
OX1	5351	RF	0.5
OX2	11156	RF	1.8
PAPP	23204	RF	5.2
PGP	6450	RF	0.5
PPB	8716	RF	0.8
PXR	37499	RF	19.8
RAT_F	6109	RF	0.5
TDI	4169	RF	0.4
THROMBIN	5100	RF	0.4
2C8	22500	DNN_STANDARD	20
2C9BIG	142000	DNN_STANDARD	167
2D6	37500	DNN_STANDARD	37.5
3A4	37499	DNN_STANDARD	38
A-II	2072	DNN_STANDARD	1.5
BACE	13101	DNN_STANDARD	9.83
CAV	37500	DNN_STANDARD	36
CB1	8730	DNN_STANDARD	6.5
CLINT	17469	DNN_STANDARD	13.84
DPP4	6150	DNN_STANDARD	4.33
ERK2	9632	DNN_STANDARD	7.67
FACTORXIA	7149	DNN_STANDARD	5.33
FASSIF	67100	DNN_STANDARD	68
HERG	37473	DNN_STANDARD	36.67
HERGBIG	238000	DNN_STANDARD	292.5
HIV_INT	1815	DNN_STANDARD	1.17
HIV_PROT	3233	DNN_STANDARD	2.5
HPLC_LOGD	37500	DNN_STANDARD	36
METAB	1569	DNN_STANDARD	1
NAV	34682	DNN_STANDARD	31.83
NK1	10050	DNN_STANDARD	7.33
OX1	5351	DNN_STANDARD	3.5
OX2	11156	DNN_STANDARD	8.17

PAPP	23204	DNN_STANDARD	20
PGP	6450	DNN_STANDARD	4.17
PPB	8716	DNN_STANDARD	6
PXR	37499	DNN_STANDARD	40.1
RAT_F	6109	DNN_STANDARD	4.67
TDI	4169	DNN_STANDARD	3.16
THROMBIN	5100	DNN_STANDARD	3.66
2C8	22500	DNN_QUICK	2.66
2C9BIG	142000	DNN_QUICK	23
2D6	37500	DNN_QUICK	5
3A4	37499	DNN_QUICK	5
A-II	2072	DNN_QUICK	0.17
BACE	13101	DNN_QUICK	1.33
CAV	37500	DNN_QUICK	4.67
CB1	8730	DNN_QUICK	0.66
CLINT	17469	DNN_QUICK	1.67
DPP4	6150	DNN_QUICK	0.5
ERK2	9632	DNN_QUICK	0.83
FACTORXIA	7149	DNN_QUICK	0.67
FASSIF	67100	DNN_QUICK	9
HERG	37473	DNN_QUICK	4.83
HERGBIG	238000	DNN_QUICK	40
HIV_INT	1815	DNN_QUICK	0.16
HIV_PROT	3233	DNN_QUICK	0.34
HPLC_LOGD	37500	DNN_QUICK	4.83
METAB	1569	DNN_QUICK	0
NAV	34682	DNN_QUICK	3.83
NK1	10050	DNN_QUICK	0.84
OX1	5351	DNN_QUICK	0.5
OX2	11156	DNN_QUICK	1
PAPP	23204	DNN_QUICK	2.5
PGP	6450	DNN_QUICK	0.5
PPB	8716	DNN_QUICK	0.67
PXR	37499	DNN_QUICK	4.83
RAT_F	6109	DNN_QUICK	0.5
TDI	4169	DNN_QUICK	0.34
THROMBIN	5100	DNN_QUICK	0.5
2C8	22500	XGBOOST_STANDARD	0.15
2C9BIG	142000	XGBOOST_STANDARD	1.2
2D6	37500	XGBOOST_STANDARD	0.28
3A4	37499	XGBOOST_STANDARD	0.266
A-II	2072	XGBOOST_STANDARD	0.017
BACE	13101	XGBOOST_STANDARD	0.05
CAV	37500	XGBOOST_STANDARD	0.25
CB1	8730	XGBOOST_STANDARD	0.05
CLINT	17469	XGBOOST_STANDARD	0.084
DPP4	6150	XGBOOST_STANDARD	0.034
ERK2	9632	XGBOOST_STANDARD	0.05
FACTORXIA	7149	XGBOOST_STANDARD	0.034
FASSIF	67100	XGBOOST_STANDARD	0.5
HERG	37473	XGBOOST_STANDARD	0.266
HERGBIG	238000	XGBOOST_STANDARD	2.05
HIV_INT	1815	XGBOOST_STANDARD	0.01
HIV_PROT	3233	XGBOOST_STANDARD	0.017
HPLC_LOGD	37500	XGBOOST_STANDARD	0.25
METAB	1569	XGBOOST_STANDARD	0.017

NAV	34682	XGBOOST_STANDARD	0.217
NK1	10050	XGBOOST_STANDARD	0.05
OX1	5351	XGBOOST_STANDARD	0.033
OX2	11156	XGBOOST_STANDARD	0.05
PAPP	23204	XGBOOST_STANDARD	0.133
PGP	6450	XGBOOST_STANDARD	0.033
PPB	8716	XGBOOST_STANDARD	0.033
PXR	37499	XGBOOST_STANDARD	0.25
RAT_F	6109	XGBOOST_STANDARD	0.033
TDI	4169	XGBOOST_STANDARD	0.017
THROMBIN	5100	XGBOOST_STANDARD	0.033
2C8	22500	LGB_ORIGINAL	0.027
2C9BIG	142000	LGB_ORIGINAL	0.481
2D6	37500	LGB_ORIGINAL	0.053
3A4	37499	LGB_ORIGINAL	0.051
A-II	2072	LGB_ORIGINAL	0.004
BACE	13101	LGB_ORIGINAL	0.014
CAV	37500	LGB_ORIGINAL	0.047
CB1	8730	LGB_ORIGINAL	0.009
CLINT	17469	LGB_ORIGINAL	0.018
DPP4	6150	LGB_ORIGINAL	0.007
ERK2	9632	LGB_ORIGINAL	0.017
FACTORXIA	7149	LGB_ORIGINAL	0.008
FASSIF	67100	LGB_ORIGINAL	0.1
HERG	37473	LGB_ORIGINAL	0.051
HERGBIG	238000	LGB_ORIGINAL	0.51
HIV_INT	1815	LGB_ORIGINAL	0.005
HIV_PROT	3233	LGB_ORIGINAL	0.005
HPLC_LOGD	37500	LGB_ORIGINAL	0.048
METAB	1569	LGB_ORIGINAL	0.003
NAV	34682	LGB_ORIGINAL	0.041
NK1	10050	LGB_ORIGINAL	0.01
OX1	5351	LGB_ORIGINAL	0.006
OX2	11156	LGB_ORIGINAL	0.011
PAPP	23204	LGB_ORIGINAL	0.027
PGP	6450	LGB_ORIGINAL	0.007
PPB	8716	LGB_ORIGINAL	0.009
PXR	37499	LGB_ORIGINAL	0.049
RAT_F	6109	LGB_ORIGINAL	0.008
TDI	4169	LGB_ORIGINAL	0.006
THROMBIN	5100	LGB_ORIGINAL	0.006
2C8	22500	LGB_STANDARD	0.045
2C9BIG	142000	LGB_STANDARD	0.293
2D6	37500	LGB_STANDARD	0.08
3A4	37499	LGB_STANDARD	0.064
A-II	2072	LGB_STANDARD	0.007
BACE	13101	LGB_STANDARD	0.024
CAV	37500	LGB_STANDARD	0.074
CB1	8730	LGB_STANDARD	0.012
CLINT	17469	LGB_STANDARD	0.032
DPP4	6150	LGB_STANDARD	0.008
ERK2	9632	LGB_STANDARD	0.019
FACTORXIA	7149	LGB_STANDARD	0.017
FASSIF	67100	LGB_STANDARD	0.14
HERG	37473	LGB_STANDARD	0.077
HERGBIG	238000	LGB_STANDARD	0.574

HIV_INT	1815	LGB_STANDARD	0.003
HIV_PROT	3233	LGB_STANDARD	0.006
HPLC_LOGD	37500	LGB_STANDARD	0.06
METAB	1569	LGB_STANDARD	0.003
NAV	34682	LGB_STANDARD	0.065
NK1	10050	LGB_STANDARD	0.013
OX1	5351	LGB_STANDARD	0.007
OX2	11156	LGB_STANDARD	0.014
PAPP	23204	LGB_STANDARD	0.045
PGP	6450	LGB_STANDARD	0.008
PPB	8716	LGB_STANDARD	0.011
PXR	37499	LGB_STANDARD	0.074
RAT_F	6109	LGB_STANDARD	0.009
TDI	4169	LGB_STANDARD	0.007
THROMBIN	5100	LGB_STANDARD	0.008

4. File size for all methods

Data set	Ntraining	METHOD	FILE_SIZE(MEGABYTES)
2C8	22500	DNN_QUICK	32.78
2C9BIG	142000	DNN_QUICK	46.833
2D6	37500	DNN_QUICK	38.825
3A4	37499	DNN_QUICK	38.8531
A-II	2072	DNN_QUICK	21.1875
BACE	13101	DNN_QUICK	25.8076
CAV	37500	DNN_QUICK	36.1236
CB1	8730	DNN_QUICK	24.3144
CLINT	17469	DNN_QUICK	26.9597
DPP4	6150	DNN_QUICK	22.187
ERK2	9632	DNN_QUICK	27.341
FACTORXIA	7149	DNN_QUICK	24.6837
FASSIF	67100	DNN_QUICK	38.9093
HERG	37473	DNN_QUICK	38.3915
HERGBIG	238000	DNN_QUICK	49.3819
HIV_INT	1815	DNN_QUICK	18.8193
HIV_PROT	3233	DNN_QUICK	25.1012
HPLC_LOGD	37500	DNN_QUICK	36.6294
METAB	1569	DNN_QUICK	19.5659
NAV	34682	DNN_QUICK	33.936
NK1	10050	DNN_QUICK	24.4629
OX1	5351	DNN_QUICK	20.4851
OX2	11156	DNN_QUICK	23.9411
PAPP	23204	DNN_QUICK	31.4834
PGP	6450	DNN_QUICK	21.0069
PPB	8716	DNN_QUICK	22.0505
PXR	37499	DNN_QUICK	37.7613
RAT_F	6109	DNN_QUICK	24.194
TDI	4169	DNN_QUICK	24.9446
THROMBIN	5100	DNN_QUICK	23.2186
2C8	22500	DNN_STANDARD	166.802
2C9BIG	142000	DNN_STANDARD	222.867
2D6	37500	DNN_STANDARD	190.919
3A4	37499	DNN_STANDARD	191.031
A-II	2072	DNN_STANDARD	120.554
BACE	13101	DNN_STANDARD	138.986
CAV	37500	DNN_STANDARD	180.142
CB1	8730	DNN_STANDARD	133.029
CLINT	17469	DNN_STANDARD	143.582
DPP4	6150	DNN_STANDARD	124.541
ERK2	9632	DNN_STANDARD	145.103
FACTORXIA	7149	DNN_STANDARD	134.502
FASSIF	67100	DNN_STANDARD	191.256
HERG	37473	DNN_STANDARD	189.19
HERGBIG	238000	DNN_STANDARD	233.036
HIV_INT	1815	DNN_STANDARD	111.105
HIV_PROT	3233	DNN_STANDARD	136.167
HPLC_LOGD	37500	DNN_STANDARD	182.16
METAB	1569	DNN_STANDARD	114.084
NAV	34682	DNN_STANDARD	171.414
NK1	10050	DNN_STANDARD	133.621
OX1	5351	DNN_STANDARD	117.751
OX2	11156	DNN_STANDARD	131.539

PAPP	23204	DNN_STANDARD	161.63
PGP	6450	DNN_STANDARD	119.833
PPB	8716	DNN_STANDARD	123.997
PXR	37499	DNN_STANDARD	186.676
RAT_F	6109	DNN_STANDARD	132.548
TDI	4169	DNN_STANDARD	135.543
THROMBIN	5100	DNN_STANDARD	128.657
2C8	22500	LGB_ORIGINAL	4.33
2C9BIG	142000	LGB_ORIGINAL	4.47
2D6	37500	LGB_ORIGINAL	4.35
3A4	37499	LGB_ORIGINAL	4.35
A-II	2072	LGB_ORIGINAL	4.17
BACE	13101	LGB_ORIGINAL	4.28
CAV	37500	LGB_ORIGINAL	4.38
CB1	8730	LGB_ORIGINAL	4.25
CLINT	17469	LGB_ORIGINAL	4.32
DPP4	6150	LGB_ORIGINAL	4.24
ERK2	9632	LGB_ORIGINAL	4.27
FACTORXIA	7149	LGB_ORIGINAL	4.26
FASSIF	67100	LGB_ORIGINAL	4.43
HERG	37473	LGB_ORIGINAL	4.38
HERGBIG	238000	LGB_ORIGINAL	4.38
HIV_INT	1815	LGB_ORIGINAL	4.21
HIV_PROT	3233	LGB_ORIGINAL	4.21
HPLC_LOGD	37500	LGB_ORIGINAL	4.39
METAB	1569	LGB_ORIGINAL	4.06
NAV	34682	LGB_ORIGINAL	4.36
NK1	10050	LGB_ORIGINAL	4.23
OX1	5351	LGB_ORIGINAL	4.23
OX2	11156	LGB_ORIGINAL	4.24
PAPP	23204	LGB_ORIGINAL	4.39
PGP	6450	LGB_ORIGINAL	4.29
PPB	8716	LGB_ORIGINAL	4.28
PXR	37499	LGB_ORIGINAL	4.21
RAT_F	6109	LGB_ORIGINAL	4.3
TDI	4169	LGB_ORIGINAL	4.3
THROMBIN	5100	LGB_ORIGINAL	4.27
2C8	22500	LGB_STANDARD	7.5
2C9BIG	142000	LGB_STANDARD	7.6
2D6	37500	LGB_STANDARD	7.6
3A4	37499	LGB_STANDARD	7.5
A-II	2072	LGB_STANDARD	5.8
BACE	13101	LGB_STANDARD	7.5
CAV	37500	LGB_STANDARD	7.6
CB1	8730	LGB_STANDARD	7.4
CLINT	17469	LGB_STANDARD	7.5
DPP4	6150	LGB_STANDARD	7.4
ERK2	9632	LGB_STANDARD	7.5
FACTORXIA	7149	LGB_STANDARD	7.5
FASSIF	67100	LGB_STANDARD	7.6
HERG	37473	LGB_STANDARD	7.5
HERGBIG	238000	LGB_STANDARD	7.7
HIV_INT	1815	LGB_STANDARD	5.3
HIV_PROT	3233	LGB_STANDARD	7.4
HPLC_LOGD	37500	LGB_STANDARD	7.6
METAB	1569	LGB_STANDARD	4.3

NAV	34682	LGB_STANDARD	7.6
NK1	10050	LGB_STANDARD	7.4
OX1	5351	LGB_STANDARD	7.4
OX2	11156	LGB_STANDARD	7.4
PAPP	23204	LGB_STANDARD	7.6
PGP	6450	LGB_STANDARD	7.6
PPB	8716	LGB_STANDARD	7.5
PXR	37499	LGB_STANDARD	7.2
RAT_F	6109	LGB_STANDARD	7.5
TDI	4169	LGB_STANDARD	7.6
THROMBIN	5100	LGB_STANDARD	7.4
2C8	22500	RF	21.6032
2C9BIG	142000	RF	135.2
2D6	37500	RF	35.6864
3A4	37499	RF	35.7536
A-II	2072	RF	1.9856
BACE	13101	RF	12.5792
CAV	37500	RF	35.5136
CB1	8730	RF	8.3696
CLINT	17469	RF	16.7552
DPP4	6150	RF	5.9024
ERK2	9632	RF	9.2432
FACTORXIA	7149	RF	6.8576
FASSIF	67100	RF	64.3664
HERG	37473	RF	35.5856
HERGBIG	238000	RF	228.483
HIV_INT	1815	RF	1.7456
HIV_PROT	3233	RF	3.0848
HPLC_LOGD	37500	RF	35.8928
METAB	1569	RF	1.5056
NAV	34682	RF	32.8352
NK1	10050	RF	9.5696
OX1	5351	RF	5.1392
OX2	11156	RF	10.7072
PAPP	23204	RF	21.872
PGP	6450	RF	6.1424
PPB	8716	RF	8.3072
PXR	37499	RF	35.7152
RAT_F	6109	RF	5.864
TDI	4169	RF	4.0016
THROMBIN	5100	RF	4.856
2C8	22500	XGBOOST_STANDARD	3.63065
2C9BIG	142000	XGBOOST_STANDARD	5.53562
2D6	37500	XGBOOST_STANDARD	3.56966
3A4	37499	XGBOOST_STANDARD	3.92686
A-II	2072	XGBOOST_STANDARD	2.25242
BACE	13101	XGBOOST_STANDARD	3.49824
CAV	37500	XGBOOST_STANDARD	4.2343
CB1	8730	XGBOOST_STANDARD	3.07639
CLINT	17469	XGBOOST_STANDARD	3.97027
DPP4	6150	XGBOOST_STANDARD	2.9671
ERK2	9632	XGBOOST_STANDARD	2.82245
FACTORXIA	7149	XGBOOST_STANDARD	2.70401
FASSIF	67100	XGBOOST_STANDARD	4.16726
HERG	37473	XGBOOST_STANDARD	4.7249
HERGBIG	238000	XGBOOST_STANDARD	6.5663

HIV_INT	1815	XGBOOST_STANDARD	2.23853
HIV_PROT	3233	XGBOOST_STANDARD	2.79185
HPLC_LOGD	37500	XGBOOST_STANDARD	5.21306
METAB	1569	XGBOOST_STANDARD	2.21297
NAV	34682	XGBOOST_STANDARD	3.78602
NK1	10050	XGBOOST_STANDARD	3.28231
OX1	5351	XGBOOST_STANDARD	3.17244
OX2	11156	XGBOOST_STANDARD	3.6773
PAPP	23204	XGBOOST_STANDARD	3.39024
PGP	6450	XGBOOST_STANDARD	3.39031
PPB	8716	XGBOOST_STANDARD	3.74311
PXR	37499	XGBOOST_STANDARD	4.34647
RAT_F	6109	XGBOOST_STANDARD	2.79703
TDI	4169	XGBOOST_STANDARD	2.86529
THROMBIN	5100	XGBOOST_STANDARD	3.02815